YIELD FUNCTIONS FOR CEMENTED SOILS USING THERMOMECHANICS

By

ZEYAD KATAB

A thesis submitted in partial fulfillment of

the requirements for the degree of

MASTER OF SCIENCE IN CIVIL ENGINEERING

WASHINGTON STATE UNIVERSITY

Department of Civil and Environmental Engineering

AUGUST 2012

To the Faculty of Washington State University

The members of the Committee appointed to examine the thesis of ZEYAD KATAB fined it satisfactory and recommend that it be accepted

Balasingam Muhunthan, Ph.D., Chair

William F. Cofer, Ph.D

Haifang Wen, Ph.D.

ACKNOWLEDGEMENT

First I would like to thank my advisor, Dr Balasingam Muhunthan. He guided and supported my academic success with generous dedication beyond expectation. I will be grateful for his taking a personal interest in my career. I will always appreciate the extraordinary knowledge he imparts so clearly and patiently.

Thank you also to Dr William Cofer and Dr Haifang Wen for granting me your confidence, endorsement, and serving as my committee.

I owe special thanks to my country Libya and university of Omar Al-Mukhtar for their financial support of my studies. Their generosity has helped me achieve my goals at Department of Civil and Environmental Engineering of Washington State University. Thanks are also due to Chris Vogel at Oxford University for his assistance with the MATLAB coding of the program used in the simulations.

Finally, thank you to my parents for instilling in me a respect and need for education from my young days.

YIELD FUNCTIONS FOR CEMENTED SOILS USING THERMOMECHANICS

Abstract

By Zeya Katab, M. S.

Washington State University

August 2012

Chair: Balasingam Muhunthan

The yield behavior of bonded and cemented soils is different from laboratory reconstituted soils. Experimental results have shown that these soils generally have yield surfaces whose shape and shift in the stress space is dependent on the amount of bonding present. Several models based on an elastic-plastic framework incorporating ideas of critical state soil mechanics have been proposed to capture this behavior. In some cases such models have been found to violate the laws for thermodynamics.

This study presents a thermomechanical formulation for developing yield functions suitable for cemented soils using thermomechanics. The formulation is based on the choice of a free energy function and a dissipation function from the beginning and ensures that no thermodynamic laws are violated. Different choices of the dissipation function are proposed to capture the characteristics of the yield surfaces of bonded soils. It is shown that the alpha-gamma model form of the dissipation function could capture the yield loci of published laboratory experimental data. It is found that the

shape and shift of the yield surfaces are controlled by the model parameters which are functions of cementation. The anisotropic dissipation function proposed is shown to be better suited to model the yield behavior of natural soils. Parametric studies conducted show that the rotation of the yield surface is controlled by the anisotropy parameter.

Table of Contents

LIST OF TABLES

Page

LIST OF FIGURES

Page

Chapter 1

Introduction

1.1 Bckground

The modern theories of constitutive laws for geomaterials, such as clays and sands can, arguably, be said to have begun with the critical state theories of Schofield and Wroth (1968) and Roscoe and Burland (1969) and the studies of particle interactions of Rowe (1962) and Horne (1965), which introduced the concept of a stress-dilatancy relation.

The critical state models are based on elasto-plastic continuum theories, which extended the concepts that had been very successful in modelling the behaviour of metals, but which incorporated the idea of the existence of critical void ratios at which the material sheared without any changes in stress and volume (Casagrande 1936). The original argument described by Schofield and Wroth started with a statement equating the applied work increment to the dissipation increment. This same relation could also be also be interpreted as a stress-dilatancy relation (Taylor 1948). They then used an argument based upon Drucker's hypothesis to deduce the shape of the yield loci and the associated flow rule; the model now known as "Original Cam Clay". This model had the unsatisfactory property of the yield loci having vertices on the pressure axis. This problem was overcome by Roscoe and Burland (1969) who modified the dissipation increment function to include volume strains, and deduced the well known "Modified Cam Clay" model with elliptical yield loci. Although this model gave improved

agreement with experimentally determined yield loci, at least for lightly over consolidated clays, its associated stress-dilatancy relation (flow rule) was less accurate than the original model. Whilst the arguments these authors used for deducing the flow rule and yield condition from a work equation was in line with elasto-plasticity theory current at the time, they can now be seen to be erroneous in the light of the modern theories of thermomechnics based elastoplasticity theory (Collins and Kelly 2002). Furthermore, the original family of critical state models were developed for laboratory reconstituted soils.

Since natural soil behaviour is different from reconstituted soils, the original "Cambridge Models" have been extended in a number of directions, including effects such as inherent and induced anisotropy, non-associated flow rules, shear hardening, bounding surfaces and kinematic hardening. However, with very few exceptions, in contrast to the original models, these extended models are often not based on any mechanical or thermomechanical principles. Here we present a thermomechanical formulation for developing constitutive models for natural and bonded soils. The model is formulated for triaxial conditions for simplicity.

1.2 Objectives of the study

The specific objectives of the study are to:

1- Develop yield functions suitable for cemented soils using thermomechanics;

2- Verify the yield surface of bonded soils from published literature, and

3- Perform parametric studies to identify the influence of factors such as bonds and friction on yielding.

1.3 Organization of the thesis

This thesis organized into four chapters. Chapter 2 gives a brief description about the models, and the yield behavior of natural soils. Chapter 3 provides a literature review of the current models; which include the Isotropic Alpha-Gamma model and the anisotropic Alpha-Gamma model. Chapter 4 presents the development of yield functions suitable for cemented soils using thermomechanics. Chapter 5 provides the summary of the main conclusion reached by this study, and makes future recommendations for future research in this area.

Chapter 2

Yield Behavior of Natural Soils

2.1 Yield behavior of clay

Several researchers have studied the effect of bonding on the yielding behavior of cemented soils (Leroueil and Vaughan 1990; Chazallon, et al. 1995; Vatsala, et al. 2001; Yong et al. 2011; Vaunat and Gens 2003). Based on laboratory studies it has been found that the presence of bonds and coupling in cemented soils result in their structural initial yield locus to be different from reconstituted soils as shown schematically in Figure 2.1. It is seen that the presence of bonds in natural soils introduces cohesion to frictional soils and tensile strength which cause enlargement of the yield surface and shift towards the left of the stress diagram. Consequently, the position of the structural yield surface is to shift the ellipse to the left side with distance p_r = C/M, where C is the cohesion and M is the frictional constant or the slope of the critical state line. During plastic shear deformation such bonds degrade and the yield surface returns to the isotropic yield surface (Gens and Nova 1993; Vatsala et al 2001). Such progressive degradation must be incorporated in a model to properly capture their effects in the stress strain behavior of cemented soils.

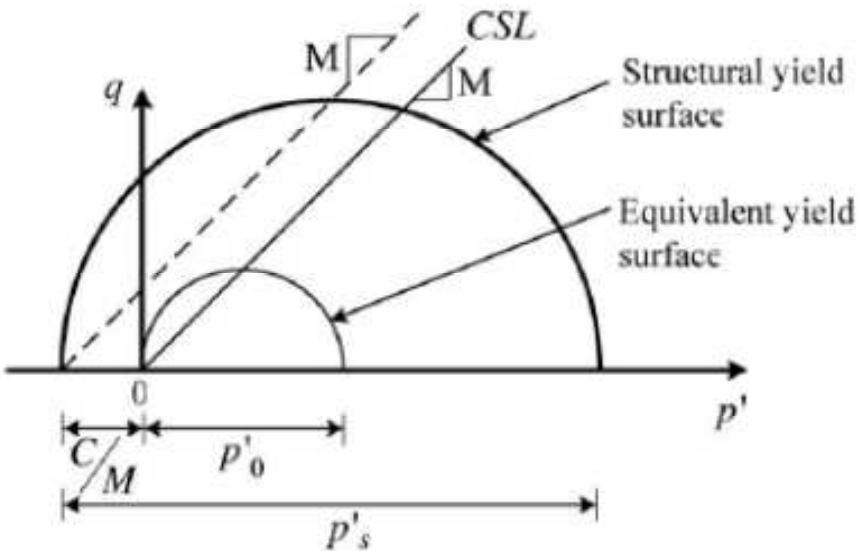

Figure 2.1: Structural and equivalent yield surfaces (after Kasama et al, 2000)

Studies have also been done on the yield behavior of natural bonded soils. It has been found that the yield behavior of these soils also followed a similar pattern as in natural clays and that it is anisotropic and rotated from the p-axis as shown in Figure 2.2. Note that the yield curve of natural soil goes through the origin whereas it is expected that for bonded soils it must be shifted following the isotropic laboratory observation above. However, the data on bonded soils is incomplete and further testing is needed to develop a comprehensive models.

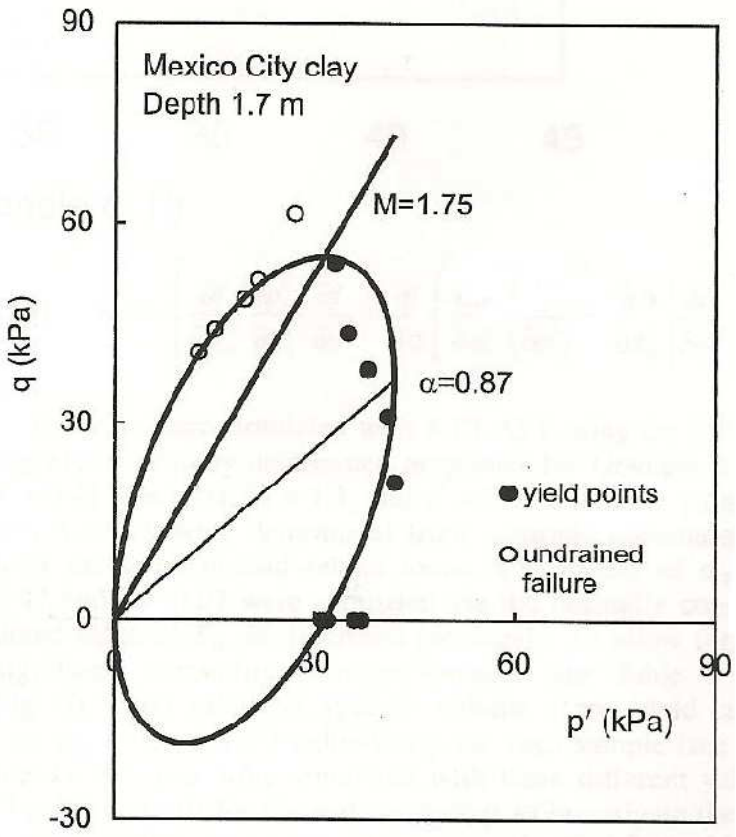

Figure 2.2: Initial yield curve for Mexico City clay (after Wheeler et al. 2003)

2.2 Laboratory Data on cemented soils

Data used in this study consists of those used by (Kasama et al, 2000). They prepared artificially cemented clay by mixing cement with clay and undrained triaxial compression tests, standard consolidation tests, and constant mean effective stress tests were performed to evaluate the effect of increasing cementation on stress - strain behaviour and strength properties. A slurry containing Portland cement was mixed with Ariake Clay (LL = 86.5%, PI = 51.3 and $\rho_s = 2.609\,g/cm^3$) in slurry two times the LL water content. In preparing the samples, cement contents of 1%, 3%, and 5% per dried sample weights were selected. Each reconstituted clay sample was consolidated in one

dimension up to 49 kPa confining pressure. A series of standard consolidation tests and undrained triaxial compression tests were performed according to the Japanese Geotechnical Society with constant mean effective stress tests.

Figure 2.3 shows the stress-strain relationships at a confining pressure of 294 kPa during undrained triaxial compression tests. It can be observed that the stress-strain relationships show a clear trend from strain hardening to post peak strain softening behavior as the cementation increases (Kasama et al, 2000)

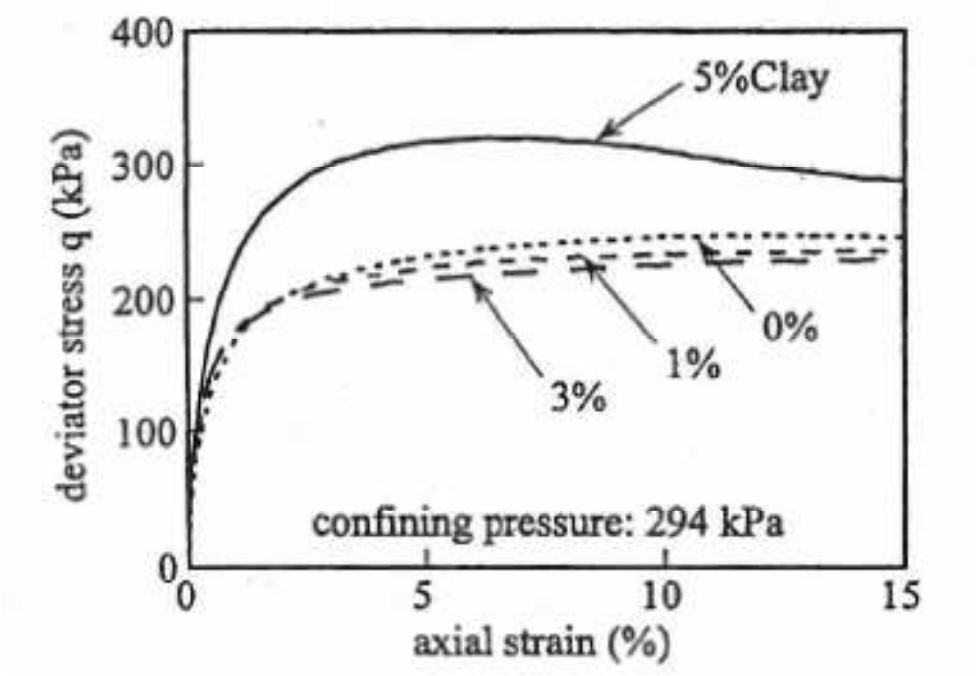

Figure 2.3: Stress-strain relationship of clay with various values of cement contents (after Kasama et al, 2000)

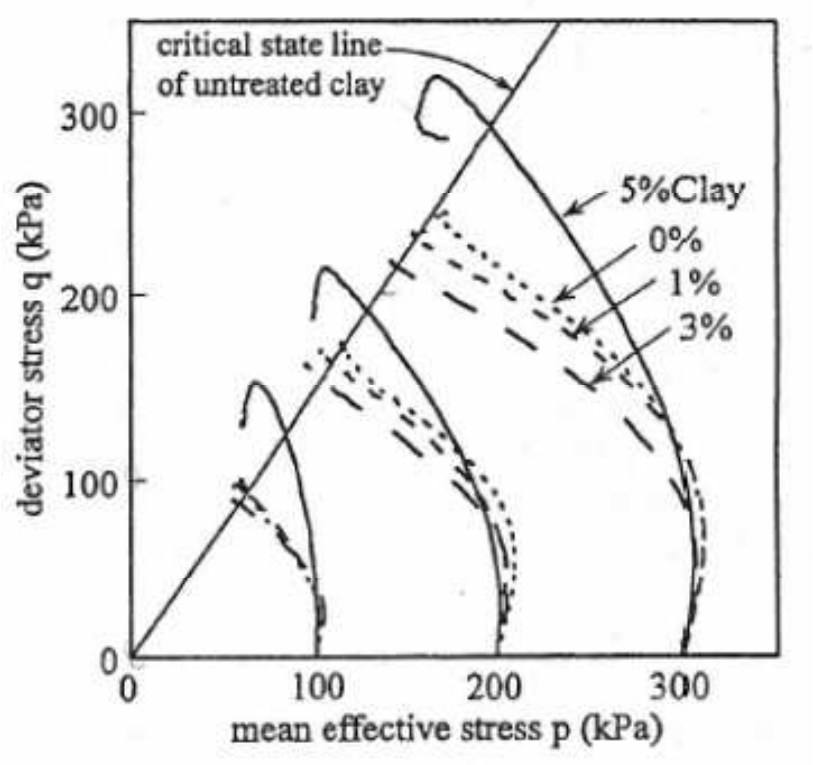

Figure: 2.4. Stress path of lightly cemented clays (after Kasama et al, 2000)

The undrained stress path in $p-q$ space is shown in Fig. 2.4. The straight line in this figure shows the critical state line of uncemented clay. It can be seen that the failure state line of lightly cemented clay is located above the critical state line on uncemented clay.

2.3 Elasto-plastic Framework

Nova and Gens (1993) discussed the basic conceptual requirements for the development of an elastic-plastic constitutive model for bonded soils within the framework of hardening plasticity. They presented a simple mathematical model, and applied some conventional laboratory tests. The yield surface was thought to have the same shape and forms as that of the uncemented soil, but was enlarged to account for

the additional strength provided by the bonds. The hardening parameter was considered to be made up of two components; the hardening of the unbounded soil, and the softening due to degradation of cementation bonds with plastic strain. They applied the model to simulate the triaxial compression tests starting from different values of mean stress. All specimens have the same initial values of $p_S = 100kPa$ and the degree of bonding $b_0 = 1$ (Fig 2.5)

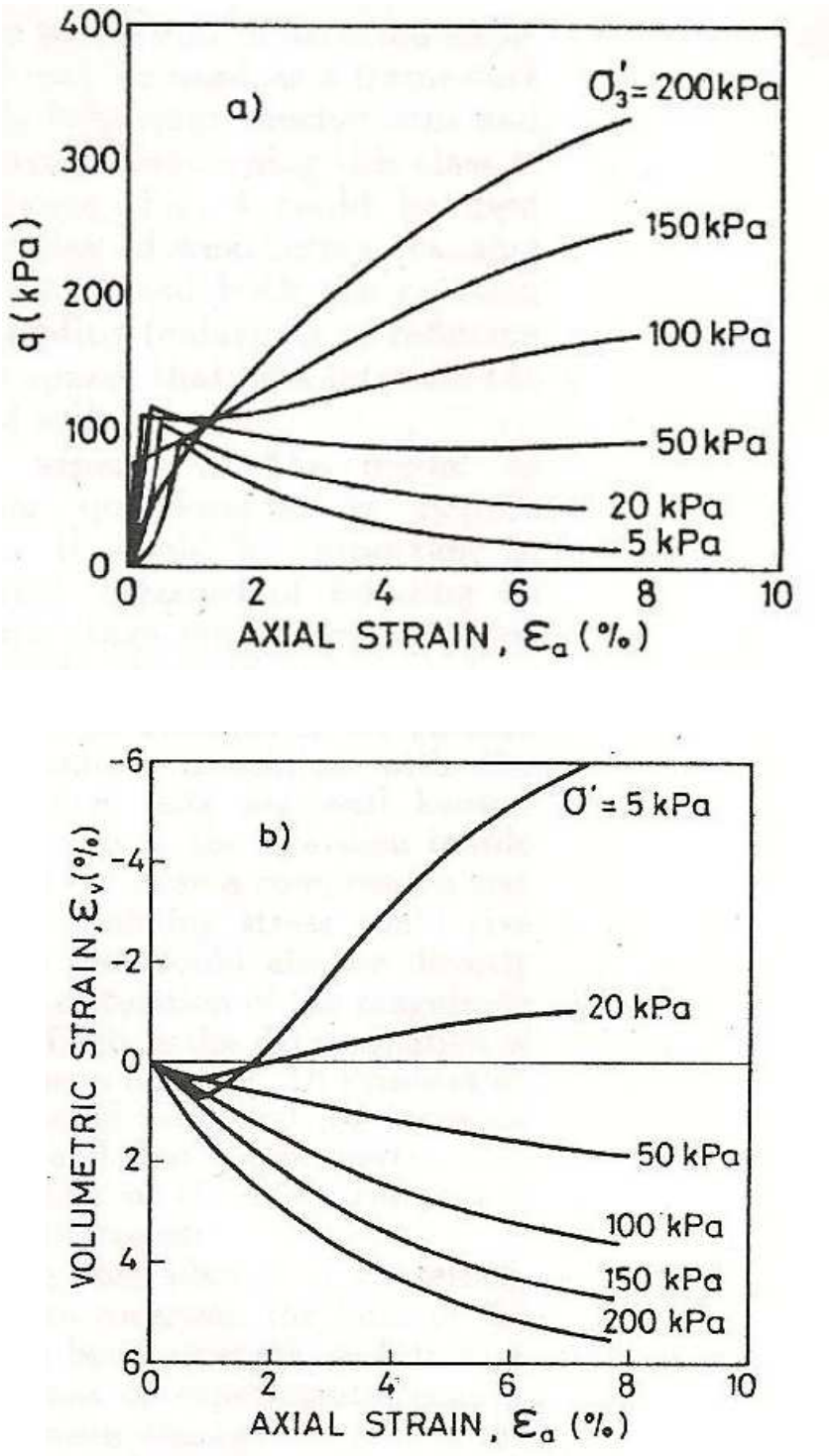

Figure 2.5: Computed triaxial compression test results (after Nova and Gens, 1993).

a) Deviator stress vs. axial strain. b) volumetric strain vs. axial strain

It can be noted that as the confining stress increases, specimens tested in shear show a transition from a brittle/dilatant behavior to a ductile/compressive behavior. Also the initial stiffness and deviator stress at yield may decrease at high confining stresses.

This study develops a thermomechanical model in Chapter 3 based on some of the ideas used in plasticity. Before describing the thermomechanical modeling framework for natural soils, it is first necessary to define the volume strains as used here.

2.4 Specific volume and volume strains.

When presenting critical state models it is usual to represent the critical state by a line in the e – ln (p), or v – ln (p) plane, where e is the voids ratio, v is the specific volume, and p is the effective pressure. At low stress levels, where grain crushing is insignificant, this line is normally taken to be straight. However, Butterfield (1979) pointed out that the experimental data, equally well, fitted a straight line in the ln(v) – ln(p) plane, and that from a modelling view-point, this had the advantage that, unlike e and v, ln(v) could be interpreted as the volume strain. This representation is becoming increasingly popular. By definition the specific volume is given by:

$$v = \Delta V / \Delta V_s \tag{2.1}$$

Where ΔV and ΔV_s are the total volume and solid volume of a continuum element. Upon differentiation we find:

$$d(\ln(v)) \equiv \frac{dv}{v} = \frac{d(\Delta V)}{\Delta V} - \frac{d(\Delta V_s)}{\Delta V_s} \tag{2.2}$$

The first term on the right hand side is the total volume strain increment de_V, so that ln(v) can be regarded as the total volume strain only if the last term is ignored. In the case of a hard grained media such as sand, the volume changes of the grains are elastic, and the last term in (2) is actually the *elastic* volume strain increment $\dot{e}_v^e$. Hence ln(v) is e_V^P the *plastic* not the *total* volume strain e_V. In many situations the elastic strain is a small fraction of the total strain and can be ignored. However there are two situations in which this is not true. One is when modelling undrained tests, where the sum of the elastic and plastic volume strains is constant and the elastic strains cannot be ignored and must be clearly identified. The other, which is relevant to the topic of this paper, is where we are concerned with energy balances. Because of the large grain stiffnesses, the associated elastic energy may well be a significant part of the applied work, despite the insignificance of corresponding strains.

Chapter 3

Thermomechanical formulations

3.1 General

Thermomechanical analyses of various aspects of models exhibiting critical states have been presented in a number of papers by Collins and Muhunthan together with various collaborators (Collins and Houlsby 1997; Collins and Kelly 2002; Collins and Muhunthan 2003, Collins et al. 2008). Here we summarize the main results.

For isothermal deformations the First and Second Laws of Thermodynamics state that the rate of working is equal to the rate of change of the free energy plus the rate of dissipation, and that the latter can never be negative. The free energy potential represents the elastic energy which is stored in the deformed grains, whilst the rate of dissipation potential describes the energy dissipated by friction during the relative sliding and rolling of the individual grains. Due to the rearrangement of the grains, not all the elastic energy is released upon unloading. The free energy is hence regarded as the sum of two terms: the “recoverable energy” term and the “frozen energy” term; the latter depending on the plastic strain, which describes the grain rearrangement (Ulm and Coussy 2003, Collins 2005 b, Li, 2007).

Using the standard notation for triaxial tests, the plastic work rate can hence be written:

$$\widetilde{W}^{P} = \dot{\Psi}^{P}(e_V^P) + \widetilde{\Phi}(\alpha, e_V^P, \dot{e}_V^P, \dot{e}_\gamma^P) \text{ where } \widetilde{\Phi} \geq 0 \qquad (3.1)$$

where Ψ^{P} is the frozen energy part of the free energy , $\widetilde{\Phi}$ is the rate of dissipation

potential, $\dot{e}_V^P$ and $\dot{e}_\gamma^P$ are the volumetric and shear components of the plastic strain, whilst α represents the, as yet unspecified, state parameter or set of state parameters.

It is assumed that the frozen free energy term Ψ^P is determined by the volumetric part of the plastic strain. This assumption proves to be equivalent to postulating the existence of a unique critical state line in the lnv – lnp plane (Collins et al. 2008). It has also been verified experimentally by Luong (1986) who showed that in shear flow all the energy is dissipated.

Introducing the appropriate work conjugate stress variables the identity (3.1) can be rewritten as:

$$p\dot{e}_V^P + q\dot{e}_\gamma^P = p_S\dot{e}_V^P + (p_D\dot{e}_V^P + q_D\dot{e}_\gamma^P) \tag{3.2}$$

where p and q are the effective pressure and triaxial shear stress, whilst the "shift pressure" p_S, the "dissipative pressure" p_D and the "dissipative shear stress" q_D are given by:

$$p_S = \frac{\partial \Psi^P(e_V^P)}{\partial e_V^P} \quad , \quad p_D = \frac{\partial \tilde{\Phi}}{\partial \dot{e}_V^P} \ , and \ q_D = \frac{\partial \tilde{\Phi}}{\partial \dot{e}_\gamma^P}, \quad \text{respectively.} \tag{3.3}$$

The first equation comes directly from Equation (3.1), whilst the latter two equations come from the application of Euler's theorem for homogeneous functions. The dissipation potential has to be homogeneous of degree one in the plastic strain rates, since the material behaviour is rate independent. We will also invoke Ziegler's orthogonality postulate (or equivalently the maximum entropy production principle). See accounts in Maugin (1992, 1999), Collins (2005a), Houlsby and Puzrin (2002) or Rajagopal and Srinavasa (1998) for a full explanation of these issues. This assumption enables us to equate like terms in equation (3.3), and deduce that:

$$p = p_S + p_D \text{, and } q = q_D \tag{3.4}$$

At the critical state, there is no volumetric dissipation and both p_D and $\dot{e}_v^P$ are zero. (Collins and Kelly 2002), and hence the critical state pressure is the shift pressure $p = p_S$.

3.2 Dissipation rate potentials and generalized critical state models

To proceed further we need to specify the dissipation function $\tilde{\Phi}$. The choice of the dissipation function has been guided by the ones that were used in the original critical state models and given by (Collins and Kelly 2002; Collins and Muhunthan 2003):

$$\tilde{\Phi} = p_S \sqrt{\dot{e}_v^{P\,2} + M^2 \dot{e}_\gamma^{P\,2}} \tag{3.5}$$

3.3 Yield Surface

In order to model a wider class of materials, the form of the dissipation function above has been modified by Collins and Hilder (2002) as:

$$\tilde{\Phi} = \sqrt{(A\dot{e}_v^P)^2 + (B\dot{e}_\gamma^P)^2} \tag{3.6}$$

Where A and B have the dimensions of stress:

$$A = a_1 p_D + a_2 q + a_3 p_S \tag{3.7}$$

$$B = b_1 p_D + b_2 q + b_3 p_S \tag{3.8}$$

Using Eqs. (3.7) and (3.8), the dissipative stresses are found to be:

$$p_D = \frac{\partial \widetilde{\Phi}}{\partial \dot{e}_V^P} = \frac{A^2 \dot{e}_V^P}{\widetilde{\Phi}} \tag{3.9}$$

$$and \quad q_D = \frac{\partial \widetilde{\Phi}}{\partial \dot{e}_\gamma^P} = \frac{B^2 \dot{e}_\gamma^P}{\widetilde{\Phi}} \tag{3.10}$$

By eliminating $\widetilde{\Phi}$ the yield surface for the dissipation function becomes:

$$\frac{p_D^2}{A^2} + \frac{q^2}{B^2} = 1 \tag{3.11}$$

The above equation is the form of an ellipse as shown in Fig 3.1.

3.4 Isotropic normal compression

The normal consolidation line (NCL) will be on the $p-$ axis when the material is under isotropic consolidation because there is no shear stress $q = 0$. This corresponds to points O and M in Fig. 3.1.

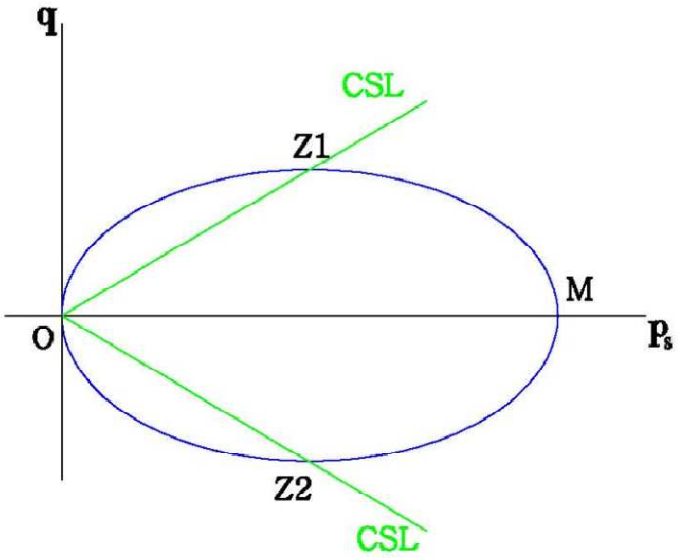

Figure 3.1: The isotropic yield surface

If the material is under isotropic compression, $\dot{e}_V^P = 0$, the shear stress is equal to zero ($q = 0$) which makes the yield surface to be:

$$\frac{p_D^{\,2}}{A^{\,2}} = 1 \tag{3.12}$$

$$p_D = \pm A \tag{3.13}$$

$$p_D = (a_1 p_D + a_3 p_S) \tag{3.14}$$

If the material under tension, $\dot{e}_V^P = 0$, so that the effective pressure equals to zero $(p = 0)$

$$p = p_D + p_S \qquad (p = 0) \tag{3.15}$$

$$p_S = -p_D \tag{3.16}$$

Substituting this equation into Eq. (3.14), we deduce that:

$$a_3 = a_1 + 1 \tag{3.17}$$

The shift pressure defined from the thermomechanics formulation is different from the conventional use of consolidation pressure in soil mechanics. They can be related by (Vogel 2010):

$$p_C = \frac{2p_S}{\gamma} \tag{3.18}$$

Where γ is a model parameter. Thus, Eq. (3.14) becomes:

$$p_C - p_S = a_1(p_C - p_S) + a_3 p_S \tag{3.19}$$

Substituting Eq. (3.18) into Eq. (3.19) results in:

$$\frac{2}{\gamma}(a_1 - 1) - a_1 + 1 + a_3 = 0 \tag{3.20}$$

Introducing parameters a_1 and a_3 as:

$$a_1 = 1 - \gamma \tag{3.21a}$$

$$a_3 = 2 - \gamma \tag{3.21b}$$

An expression for the parameter A results in:

$$A = (1-\gamma)p_D + a_2 q + (2-\gamma)p_S \tag{3.22}$$

3.5 Critical state line

At the critical state line, $\dot{e}_V^P = 0$, so the dissipative pressure is equal to zero ($p_D = 0$). Since $p_D = 0$, and $p = p_S$, the critical state line (CSL) will pass through the points Z_1 and Z_2 as shown in Fig 3.1.

The shear stress at critical state is q_{Cr} Thus, using Eq. (3.11) the parameter B becomes:

$$q_{Cr} = \pm B \tag{3.23}$$

The slope of the critical state line is:

$$M = \frac{q_{Cr}}{p_S} \tag{3.24}$$

At the critical state Eq. (3.8) results in:

$$q_{Cr} = B = b_2 q + b_3 p_S \tag{3.25}$$

Eliminating q_{Cr} using Eqs. (3.24) and (3.25)

$$Mp_S = b_2 q + b_3 p_S \tag{3.26}$$

$$Mp_S = B = b_2 (Mp_S) + b_3 p_S \tag{3.27}$$

Eq. (3.27) can be split into:

$$M = \frac{b_3}{1 - b_2} \qquad \text{If } q_{Cr} = B \tag{3.28a}$$

$$M = \frac{b_3}{1+b_2} \qquad \text{If } q_{Cr} = -B \tag{3.28b}$$

From Eqs. (3.28a), and (3.28b), we find that $b_2 = 0$, so $b_3 = M$

Since the coefficient b_1 is related to M Collins and Kelly (2002) have introduced the dimensionless parameter α, which is assumed to vary linearly between 0 and 1, to relate them:

$$b_1 = (1-\alpha)M \tag{3.29}$$

By using Eqs. (3.8), and (3.29) B can be written as:

$$B = (1-\alpha)Mp_D + Mp_S \tag{3.30}$$

Since $p_D = p - p_S$, using Eq. (3.18):

$$p_S = p - \frac{1}{2}\gamma\ p_C$$

Hence the yield condition in dissipative stress space, which represents an ellipse, can be illustrated as:

$$\frac{(p-0.5\gamma\ p_C)^2}{A^2} + \frac{q^2}{B^2} = 1 \tag{3.31}$$

Because the yield condition has an elliptical shape, the parametric angle, ω can be introduced to describe the yield surface, where

$$q = B\cos\omega \tag{3.32a}$$

$$p_D = A\cos\omega \tag{3.32b}$$

By using the linear expression for A and B, it is possible to determine the following equations (Collins and Hilder, 2002).

$$p_D(1 - a_1\cos\omega) - qa_2\cos\omega - p_S a_3\cos\omega = 0 \tag{3.33}$$

$$p_D b_1\sin\omega - q + p_S b_3\sin\omega = 0 \tag{3.34}$$

p_D *and* q can be solved by using Eqs. (3.33) and (3.34).

$$p_D = \frac{p_S(a_3 + a_2 b_2\sin\omega)\cos\omega}{1 - (a_1 + a_2 b_1\sin\omega)\cos\omega} \tag{3.35}$$

$$q = \frac{p_S((a_3 b_1 - a_1 b_3)\cos\omega + b_3)\sin\omega}{1 - (a_1 + a_2 b_2\sin\omega)\cos\omega} \tag{3.36}$$

3.6 Flow rule

The flow rule describes the relationship between the plastic strain increments, and the stress ratio.

Rewriting Eqs. (3.9) and (3.10) $\dot{e}_V^P = \frac{p_D\Phi}{A^2}$ and $\dot{e}_\gamma^P = \frac{q\Phi}{B^2}$

Thus $\frac{\dot{e}_V^P}{\dot{e}_\gamma^P} = \frac{p_D}{A^2}\frac{B^2}{q}$ (3.37)

Using Eqs. (3.32a) and (3.32b), the plastic flow rule can be obtained as:

$$\frac{\dot{e}_V^P}{\dot{e}_\gamma^P} = \frac{B\cos\omega}{A\sin\omega} \tag{3.38}$$

3.7 Hardening rule

The hardening rule describes the expansion of the yield surface with plastic deformation. The consolidation pressure is a function of the elastic volume strain and plastic volume strain, but Collins and Hilder (2002) have argued that the consolidation pressure should depend only on the volumetric plastic strain. A linear relationship between the logarithm of the consolidation pressure and the plastic strain (Collins and Hilder, 2002) is assumed. Accordingly:

$$-\ln v = e_V^P = (\lambda - k)\ln(\frac{p_S}{p_0}) \tag{3.39}$$

where λ is the slope of normal consolidation line (NCL), and k is the slope of unloading reloading line (URL) as shown in Fig 3.2.

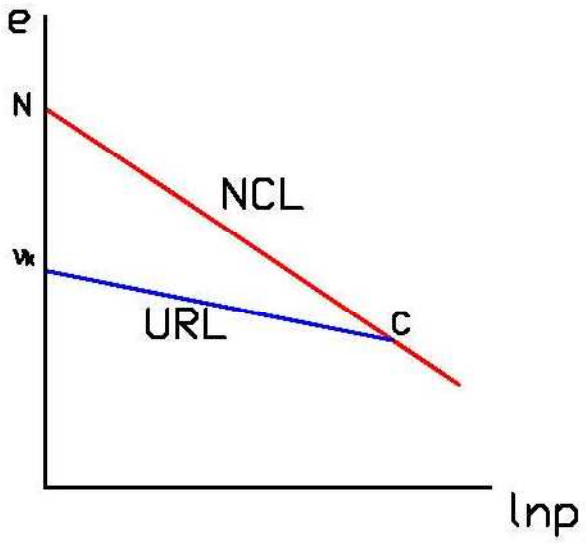

Figure 3.2: e – lnp curve

3.8 Undrained path

The undrained condition is theoretically defined as the condition in which there is no change in the fluid mass of the porous material (Sulem, 2010). An undrained test in the laboratory is performed by closing the valves of the drainage system, and subjecting the granular material to a vertical compressive stress and an isotropic horizontal pressure. It is assumed that the pore water is incompressible, so the total volume increment in an undrained test is zero.

$$\dot{e}_V = \dot{e}_V^e + \dot{e}_V^P = 0 \tag{3.40}$$

Since $$\dot{e}_V^P = -k\frac{\dot{p}}{p} \tag{3.41a}$$

and $$\dot{e}_V^e = k\frac{\dot{p}}{p} \tag{3.41b}$$

Then $\dot{e}_V^P = -k\dfrac{\dot{p}_D + \dot{p}_S}{\dot{p}_D + \dot{p}_S}$ and

$$(p_D + p_S)\dot{e}_V^P + k\dot{p}_D + k\dot{p}_S = 0 \tag{3.42}$$

Using different values for the parameters alpha α and gamma γ, the above formulation can be used to capture the yield surfaces of various granular materials.

3.9 Mathematical model

The relevant equations derived above have been combined to describe the undrained behavior of granular media. A solver has been implemented using the

ODE45 function for solving initial value ordinary differential equations in Math Works MATLAB R2009b. The quantities $p_{D,}$ p_S and q are non dimensionalized using the initial shift pressure p_{SO}. The non- dimensionalization allows the results to be easily scaled between materials (Vogel, 2010)

$$\rho = \frac{p_D}{p_{SO}},\ \xi = \frac{q}{p_{SO}}, \text{ and } \mu = \frac{p_S}{p_{SO}} \tag{3.43}$$

Thus, the system which has been solved is:

$$\begin{bmatrix} 1-a_1\cos\omega & -a_2\cos\omega & -a_3\cos\omega & A\sin\omega & 0 \\ b_1\sin\omega & -1 & b_3\sin\omega & B\cos\omega & 0 \\ 0 & 0 & 0 & 0 & A\sin\omega \\ 0 & 0 & \lambda-k & 0 & -\mu \\ k & 0 & k & 0 & \rho+\mu \end{bmatrix} \begin{bmatrix} \dot{\rho} \\ \dot{\xi} \\ \dot{\mu} \\ \dot{\omega} \\ \dot{e}_v^p \end{bmatrix} = \begin{bmatrix} 0 \\ 0 \\ B\cos\omega \\ 0 \\ 0 \end{bmatrix} e_\gamma^p \tag{3.44}$$

The MATLAB code for the above formulations is provided in Appendix A.

3.10 Model performance

The effect of varying γ on the yield loci is shown in Figs. 3.3 and 3.4. It can be seen that using smaller values of γ corresponds to the consolidation pressure being much larger than the shift pressure. On the other hand, as γ increases, the yield surface becomes slender and the shift pressure increases.

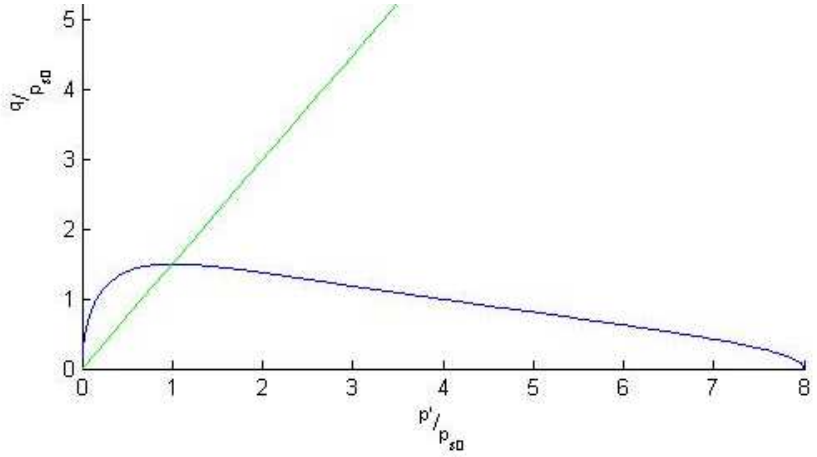

Figure 3.3: The yield loci when $\gamma = 0.25$

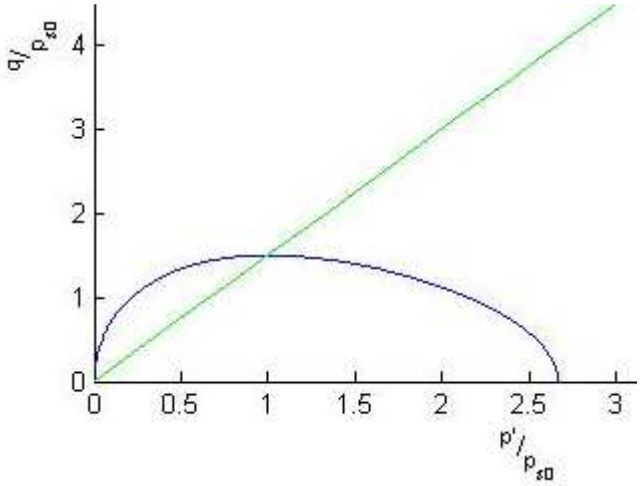

Figure 3.4: The yield loci when $\gamma = 0.75$

The effect of the α parameter on the shape of yield surface is shown in Figs 3.5 and 3.6. It can be seen that decreasing α results in a greater proportion of the dissipative stress q_D contributing to the shear strain dissipation. In addition, decreasing α values result in yield loci becoming 'tear-shaped'.

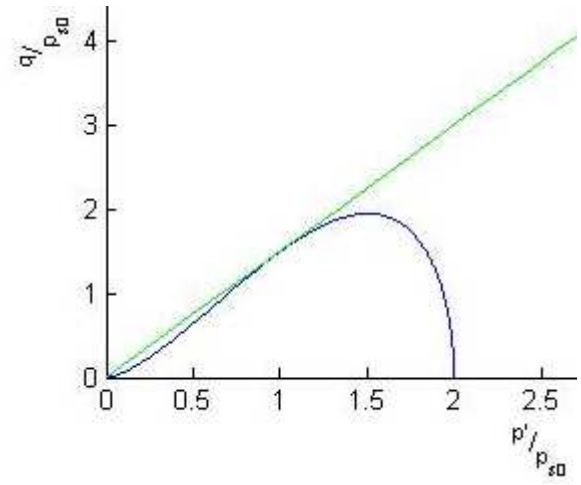

Figure 3.5: The yield loci when $\alpha = 0$

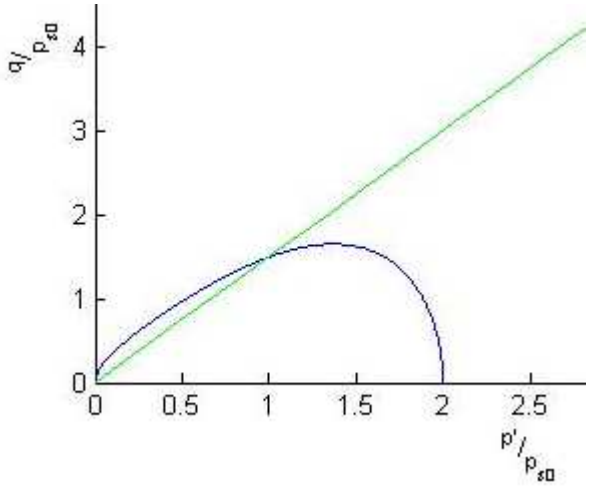

Figure 3.6: The yield loci when $\alpha = 0.5$

The above model calculations show that varying the alpha (α) and gamma (γ) parameters can be used to control the shapes of yield loci. Comparing Figures 3.3- 3.6 with Figure 3.1, it is evident that we can model the effect of bonds in natural soils by

accounting for the shifting of the pressure values with various C/M parameters. See Fig 2.1.

3.11 Anisotropic Alpha-Gamma Model

Many natural materials exhibit anisotropic behavior, which results in the directional dependence of the physical properties. Studies have shown that the anisotropy of soils results in the coupling of shear and volumetric strains during deformation. Collins and Muhunthan (2003) illustrated that the plastic volume strain increment resulted from the sum of plastic volume strain due to changes in the frozen elastic energy and dissipation related to grains rolling over each other, e_{VC}^{p} , and plastic volume strain, e_{vi}^{p} induced by shear deformation.

They assumed that the change rate of shear induced plastic strain is linearly related to the shear strain rate e_{γ}^{p} .

$$\dot{e}_{vi}^{P} = -\tan\theta * \dot{e}_{\gamma}^{p} \tag{3.45}$$

where θ is the shear induced dilatancy angle.

It is known that:

$$\dot{e}_{V}^{P} = \dot{e}_{VC}^{P} + \dot{e}_{Vi}^{P} \tag{3.46}$$

By using Eq. (3.45), equation 3.46 can be rewritten as:

$$\dot{e}_{VC}^{P} = \dot{e}_{V}^{P} + \tan\theta\ \dot{e}_{\gamma}^{P} \tag{3.47}$$

In order to account for the kinematic nature of Reynolds dilation in the plastic rate of work, $\dot{e}_{V}^{p}$ and $\dot{e}_{VC}^{p}$ should be replaced in the free energy and dissipation potentials to ensure zero-valued work (Collins et al 2008):

$$p\dot{e}_V^P + q\dot{e}_\gamma^p = p_S\dot{e}_{VC}^P + (p_D\dot{e}_{VC}^P + q_D\dot{e}_\gamma^P) + (p_r\dot{e}_{Vi}^P + q_r\dot{e}_\gamma^P) \tag{3.48}$$

Where: $p_r\dot{e}_{Vi}^P + q_r\dot{e}_\gamma^P = 0$

Hence: $$\frac{q_r}{p_r} = \tan\theta \tag{3.49}$$

And $$p = p_r = p_S + p_D \tag{3.50}$$

$$q = q_r + q_D \tag{3.51}$$

The strength ratio becomes:

$$\eta = \frac{q}{P} = \frac{q_r}{P} + \frac{q_D}{P}$$

$$\eta = \tan\theta + \frac{q_D}{P} \tag{3.52}$$

Collins and Muhunthan (2003) have argued that the strength ratio is the same astwo Coulomb-type models, which result from the resistance to rearrangement and friction.

Hence, the shift pressure, dissipative pressure, and the dissipative stress may be rewritten as:

$$p_S = \frac{\partial\Psi^P(e_{VC}^P)}{\partial e_{VC}^P} \tag{3.53a}$$

$$p_D = \frac{\partial\tilde{\Phi}}{\partial\dot{e}_{VC}^P} \tag{3.53b}$$

And, $$q_D = \frac{\partial\tilde{\Phi}}{\partial\dot{e}_\gamma^P} \tag{3.53c}$$

3.12 Yield surface

The shift and dissipative pressures are related to the compressive volumetric strain, and the dissipative shear stress is related to shear strain. Substituting Eq. (3.47) in the isotropic dissipation function gives the anisotropic dissipation function.

$$\widetilde{\Phi} = \sqrt{(A(\dot{e}_v^P + \tan\theta \dot{e}_\gamma^P))^2 + (B\dot{e}_\gamma^P)^2} \tag{3.54}$$

The dissipative stress components may be written as:

$$p_D = \frac{A^2(\dot{e}_V^P + \tan\theta \dot{e}_\gamma^P)}{\widetilde{\Phi}} \tag{3.55a}$$

$$q_D = p_D \tan\theta + \frac{B^2 \dot{e}_\gamma^P}{\widetilde{\Phi}} \tag{3.55b}$$

From which it follows that:

$$\frac{q - p_D \tan\theta}{B^2} = \frac{\dot{e}_\gamma^P}{\widetilde{\Phi}} \tag{3.56}$$

By eliminating the plastic strain increments between Eqs. (3.53) and (3.55):

$$\frac{p_D^2}{A^2} + \frac{(q - p_D \tan\theta)^2}{B^2} = 1 \tag{3.57}$$

3.13 Normal consolidation line

Following the procedure outlined in the alpha-gamma model, it is known that θ is the slope of the normal consolidation line NCL (Fig 3.7), and that the shear strain increment is zero on the current NCL.

The shift stress coefficients should be introduced as: $q_S = p_S \tan\theta$ (3.58)

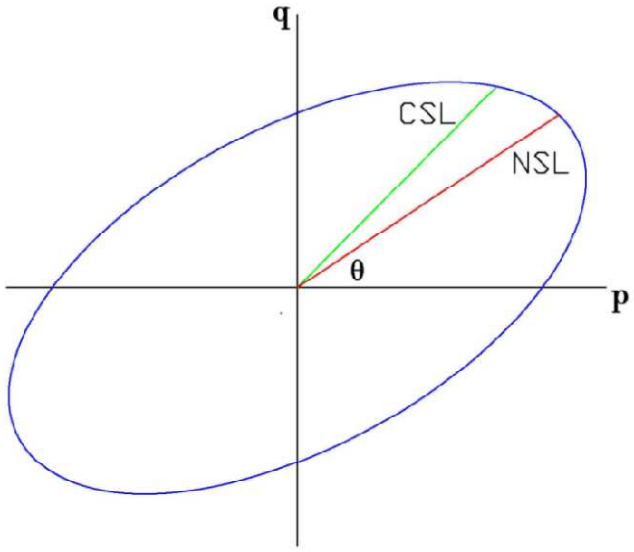

Figure 3.7: Anisotropic yield surface

So, A can be represented by the linear function of stress parameters.

$$p_D = {}^{+}_{-}\, A = {}^{+}_{-}\, (a_1 p_D + a_2 q + a_3 p_S) \tag{3.59}$$

We know that the volumetric strain increment is zero, so $q = 0$. Also the granular media have no cohesion, so in tension it gives yield at zero pressure $p = 0$.

Hence: $p_D = -p_S$

So, it can be found that: $a_3 = 1 + a_1$ (3.60)

By using maximum compression, $p_C = p_D + p_S$

Equation 3.59 can be given as:

$$p_C - p_S = (a_1 (p_C - p_S) + a_2 q + a_3 p_S) \tag{3.61}$$

From which the following is obtained:

$$a_1 = 1 - \gamma - a_2 \tan\theta \tag{3.62a}$$

$$a_3 = 2 - \gamma - a_2 \tan\theta \tag{3.62b}$$

So, the coefficient A would be:

$$A = (1 - \gamma - a_2 \tan\theta) p_D + a_2 q + (2 - \gamma - \tan\theta) p_D \tag{3.63}$$

Also, $q_D = {}^{+}_{-}\, B$

Since $p_D = 0$, $q_D = {}^{+}_{-}\, (b_2 q + b_3 p_S)$ (3.64)

The dilation angle is defined as:

$$\tan\psi = -\frac{\dot{e}_V^P}{\dot{e}_\gamma^P} = \tan\theta - \frac{B}{A}\cot\omega \tag{3.65}$$

The parametric angle ω describes the yield surface, so by using the parametric representation, p_D and q_D can be given by:

$$p_D = A\cos\omega \tag{3.66a}$$

$$q_D = A\cos\omega * \tan\theta + B\sin\omega \tag{3.66b}$$

3.14 Flow rule and hardening rule

It is clear that the flow rules in isotropic and anisotropic models are different. The anisotropic plastic flow rule is introduced:

$$A\sin\omega\dot{e}_V^P - (B\cos\omega - A\tan\theta\sin\omega)\dot{e}_\gamma^P = 0 \tag{3.67}$$

It is known that to find the anisotropic hardening rule, isotropic and kinematic hardening rules should be considered. The relation between the shift stress components can be rewritten in terms of the plastic energy function:

$$\frac{\dot{\Psi}^P}{\dot{e}_\gamma^P} = \tan\theta \frac{\dot{\Psi}^P}{\dot{e}_V^P} \tag{3.68}$$

The method of characteristics may be used to solve the first order partial differential equation for $\Psi^P(e_V^P, e_\gamma^P)$ (Collins and Hilder, 2002). Comparing the standard procedure with the differential identity:

$$\dot{e}_\gamma^P(\partial\Psi^P / \partial e_\gamma^P) + \dot{e}_V^P(\partial\Psi^P / \partial e_V^P)\tan\theta = \dot{\Psi}^P \tag{3.69}$$

It is deduced that $\dot{\Psi}^P = 0$, thus the plastic part of the free energy function remains constant along the characteristic curves in the (e_γ^P, e_V^P) which is determined by the ordinary differential equation:

$$\frac{\dot{e}_V^P}{\dot{e}_\gamma^P} = -\tan\theta \tag{3.70}$$

Collins and Hilder (2002) assumed that the rotation angle depends on plastic shear strain to model rotational hardening, from which the rotational hardening law follows:

$$\tan\theta = F'(e_\gamma^P) \tag{3.71}$$

Substituting Eq. (3.71) into (3.70) gives

$$e_V^P + F(e_\gamma^P) = C \tag{3.72}$$

The plastic part of the free energy function is introduced:

$$\Psi^P(e_V^P, e_\gamma^P) = \Psi^P(e_V^P + F(e_\gamma^P), 0) = (\lambda - k)P_0 \exp((e_V^P + F(e_\gamma^P))/(\lambda - k)) \tag{3.73}$$

Hence, the shift pressure is given as

$$p_S = p_O \exp((e_V^P + F(e_\gamma^P))/(\lambda - k))$$

$$or(\lambda - k)\ln\frac{p_S}{p_O} = \dot{e}_V^P + F(e_\gamma^P) \tag{3.74}$$

Based on some tests on sand Zienkiewicz (1999) introduced exponential decay for the variation of the anisotropy parameter:

$$\tan\theta = \tan\theta_f(1 - \exp(-\beta e_\gamma^P)) \tag{3.75}$$

Hence, $$F(e_\gamma^P) = \tan\theta(e_\gamma^P + \frac{1}{\beta}(\exp(-\beta e_\gamma^P) - 1)) \tag{3.76}$$

Where the dilation angle increases from zero to the final value θ_f.

3.15 Undrained path

As discussed before, the total volume of a representative volume element does not change, thus the undrained loading path is given as:

$$(p_D + p_S)\dot{e}_V^P + k\dot{p}_D + k\dot{p}_S = 0 \tag{3.77}$$

The anisotropic model introduces the induced dilation angle to the isotropic model. The effect of varying θ is shown in Figs 3.8 and 3.9.

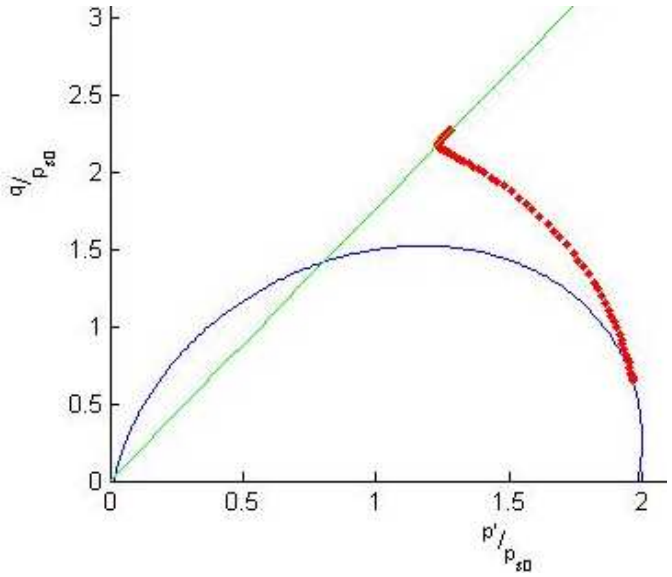

Figure 3.8: The yield loci when $\theta = 15$

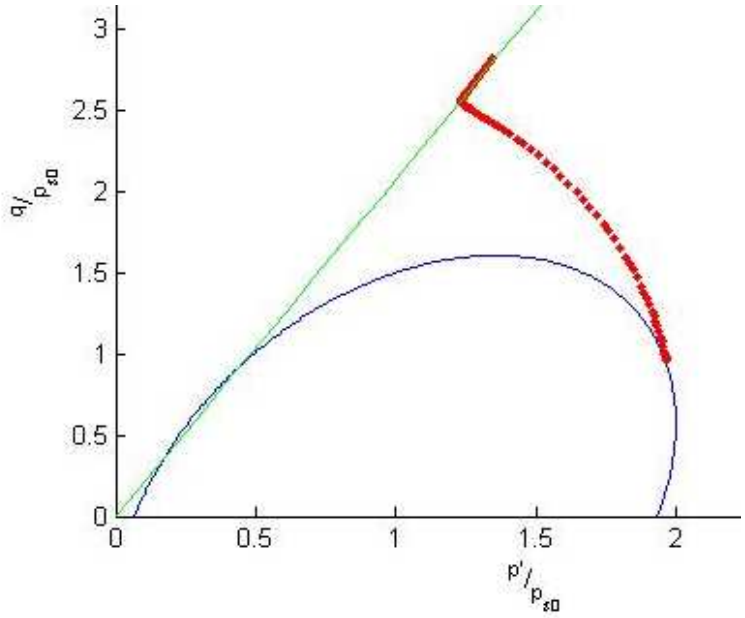

Figure 3.9: The yield loci when $\theta = 30$

Chapter 4

Simulation of Yield Surfaces

4.1 General

This chapter presents first results of the simulation of the observed yield surfaces using the alpha-gamma model from laboratory tests on cemented soils. The analyses are extended for the anisotropic model and comparisons are made of the two predictions.

4.2 Alpha-gamma model simulation of laboratory tests

The yield and undrained paths of laboratory consolidated cemented clays for various percentages of cement obtained by Kasama et al. (2000) were presented in Chapter 2 (Fig 2.4). The percentages of cement considered were 1%, 3%, and 5% per dry sample weights (Table 4.1). The relevant soil parameters are shown in Table 4.1.

Table 4.1: Soil constants of lightly cemented clay

Cement content	λ	k	Slope M	$p_r = C/M$ (kPa)
0%	1.166	0.034	1.49	0
1%	1.166	0.034	1.49	8
3%	1.166	0.034	1.49	15
5%	1.166	0.034	1.49	47

Since the yield surface is shifted to the negative axis in bonded soils, the yield surface formulation of the model proposed in Chapter 3 is modified by a variable $p_{S+}p_r$ where $p_r = C/M$ (See. Fig.2.4) is the parameter. The p_r values obtained from test data are given in Table 4.1.

In order to predict the observed yield surfaces and the corresponding undrained paths, the values of γ were varied by trial and error until a match was obtained as shown in Figure 4.1. It was found, for example, that a value of γ = 0.73 fits the yield surface corresponding to 3% cement content.

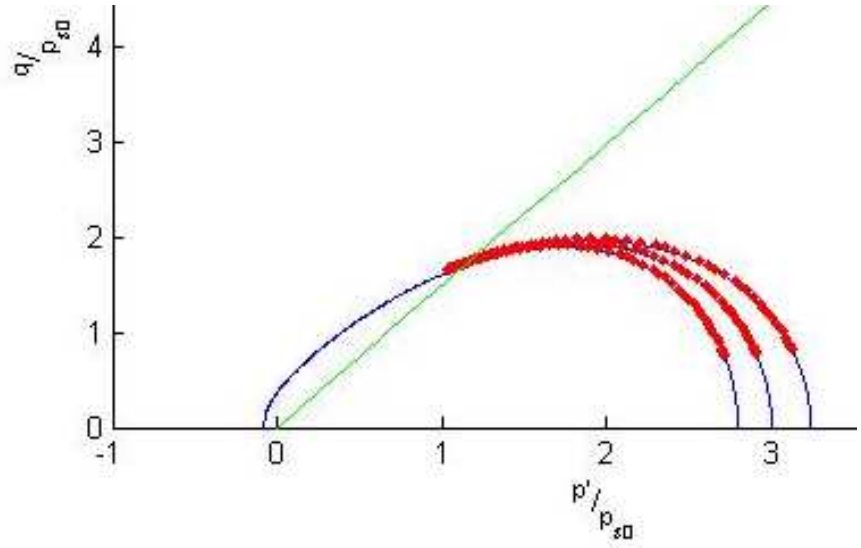

Figure 4.1: The yield surface when $p_r = 3\%$ and $\gamma = 0.75,\ 0.73,\ and\ 0.7$

The analyses were repeated for other cement contents and the results are as shown in Figures 4.2 to 4.4. It is evident that the cement content has a direct influence on the shift of the yield surface on the negative side as well as its expansion. The values of γ for the different cement percentages are tabulated in Table 4.2 and the variation is

plotted in Figure 4.5. It is apparent that the γ parameter is linearly related to the cement percentage.

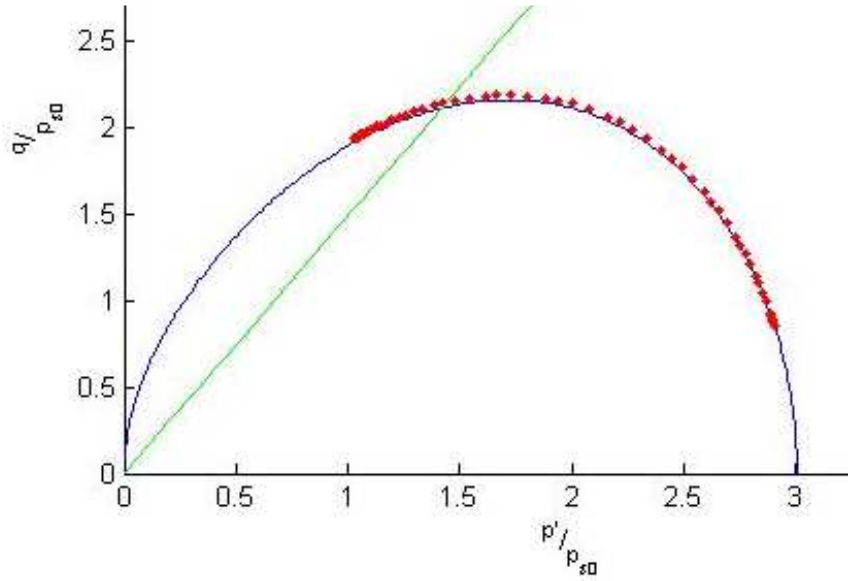

Figure 4.2: The isotropic yield surface with 0% cement content

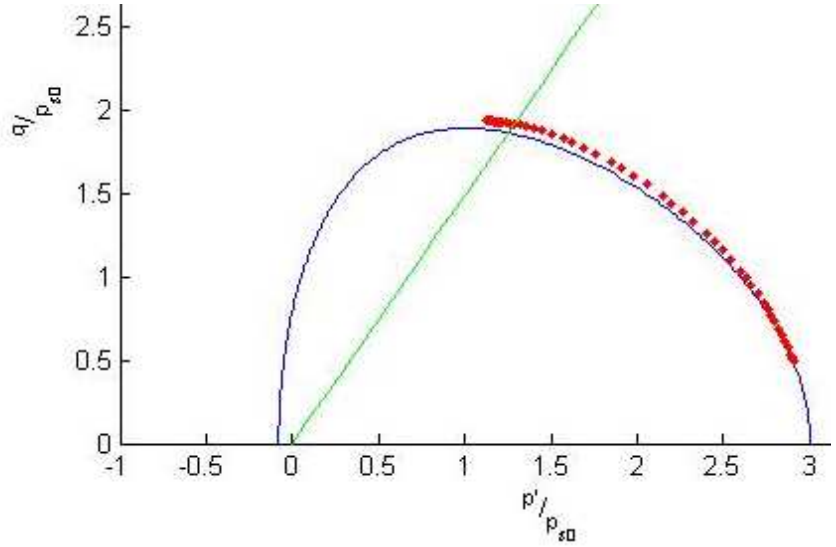

Figure 4.3: The isotropic yield surface with 1% cement content

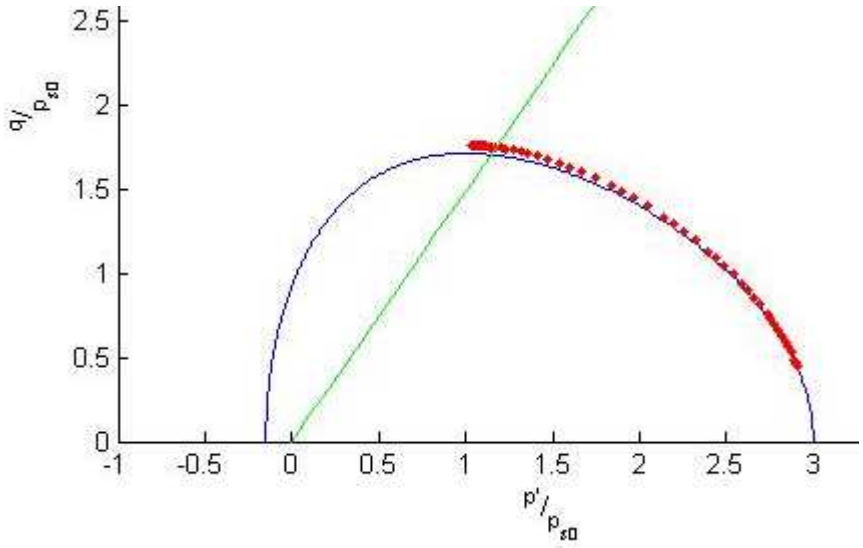

Figure 4.4: The isotropic yield surface with 3% cement content

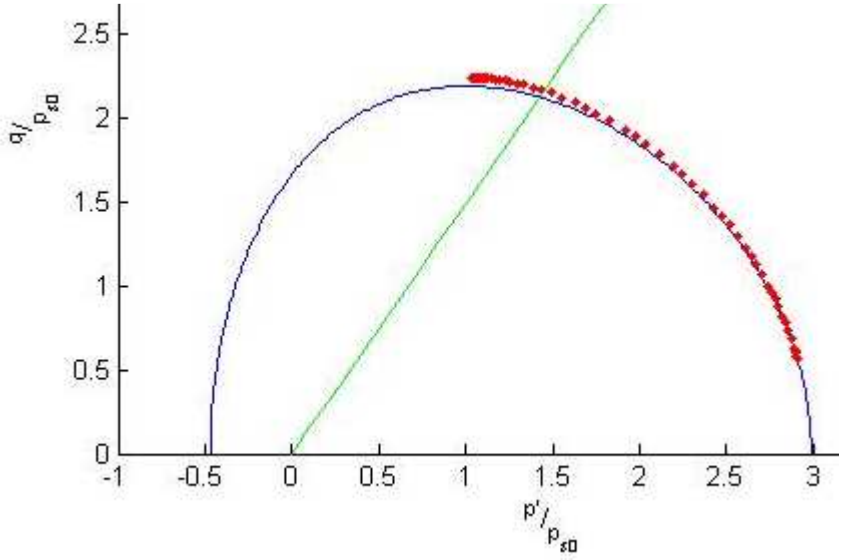

Figure 4.5: The isotropic yield surface with 5% cement content

Table 4.2 : Cement content vs gamma

Cement content	p_r %	γ
0%	0	0.665
1%	0.08	0.7
3%	0.15	0.73
5%	0.47	0.85

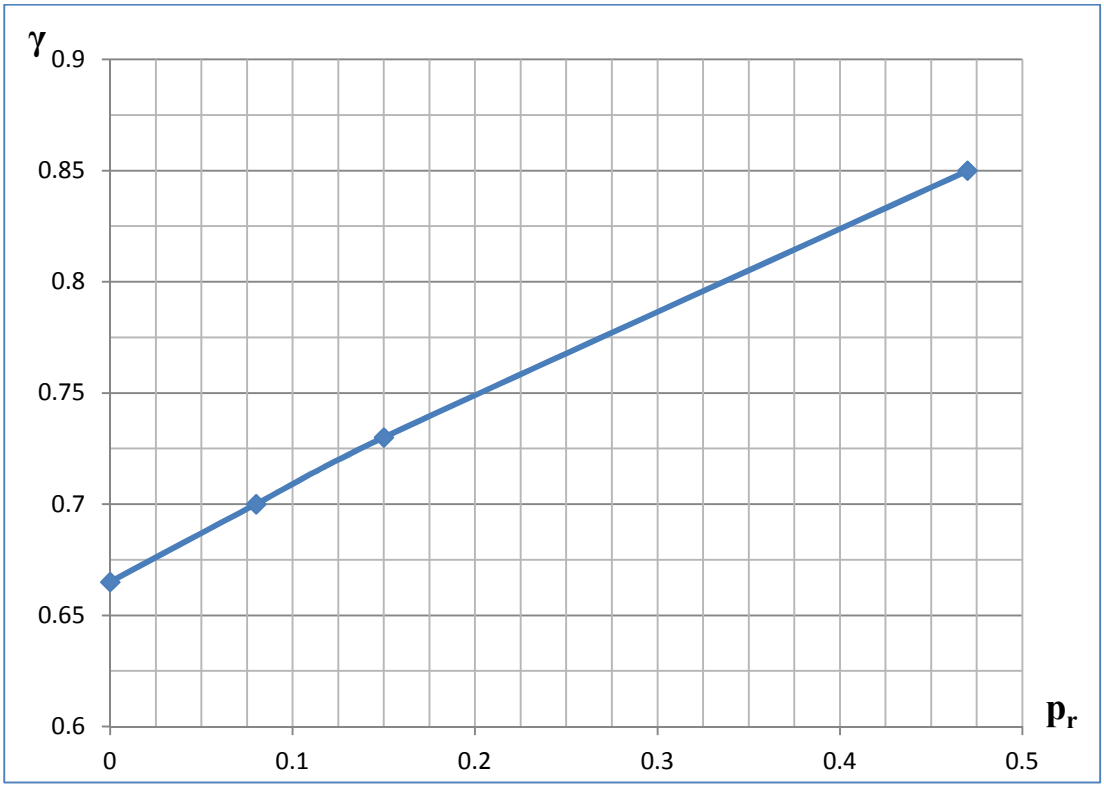

Figure 4.6: Gamma variation with p_r

4.3 Simulation of anisotropic yield surface

While experimental results on yield behavior are available for natural soils (see Muhunthan et al. 1997), to the author's knowledge few good data exist on the yield behavior of natural bonded soils. Since the yield surfaces of natural clays are rotated generally along the K_0 –axis, Muhunthan et al. (1997) used an anisotropic elastic-plastic model based on critical state energy dissipation ideas to successfully model them. This model assumed a coupling between shear and volumetric strain as done here in the thermomechanics based anisotropic model in Chapter 3 (See Eq. 3.45). The success of the elastic plastic model encouraged the author to look at the application of the anisotropic thermomechanical model to simulate the yield surfaces and undrained paths of natural bonded soils and the results of a parametric study are shown here.

In the anisotropic yield model the dilatancy angle has an effect on the undrained path (Eq 3.77), and the critical state line. In order to simulate this, a constant value of γ =1 is first assumed and dilatancy angles θ= 0, 10, and 20 were used. The results are as shown in Fig 4.7. It is seen that that the undrained path increases with an increase of the dilatancy angle, as does the slope of the critical state line.

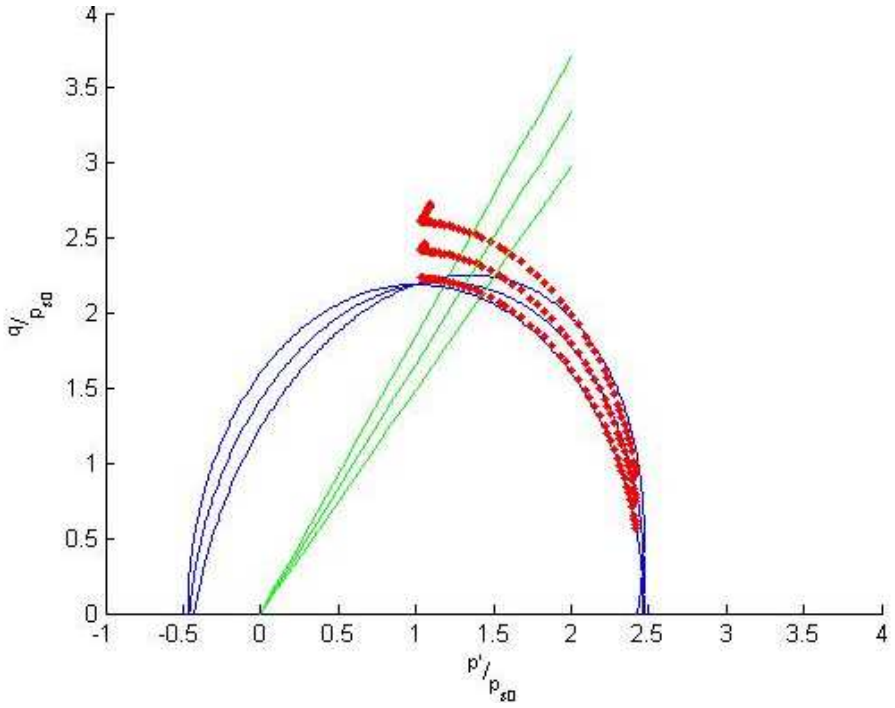

Figure 4.7: Anisotropic yield surface and undrained path when $\gamma = 1$ and $\theta = 0,\ 10,\ and\ 20$

A second series of analyses was conducted by keeping the shear induced dilatancy angle constant and varying the γ parameter. The results are as shown in Figure 4.8. It is seen that increasing in the γ parameter corresponds to an increase in the degree of cementation. Note that this is similar to what was found earlier in the simulation using an isotropic model (Fig. 4.6).

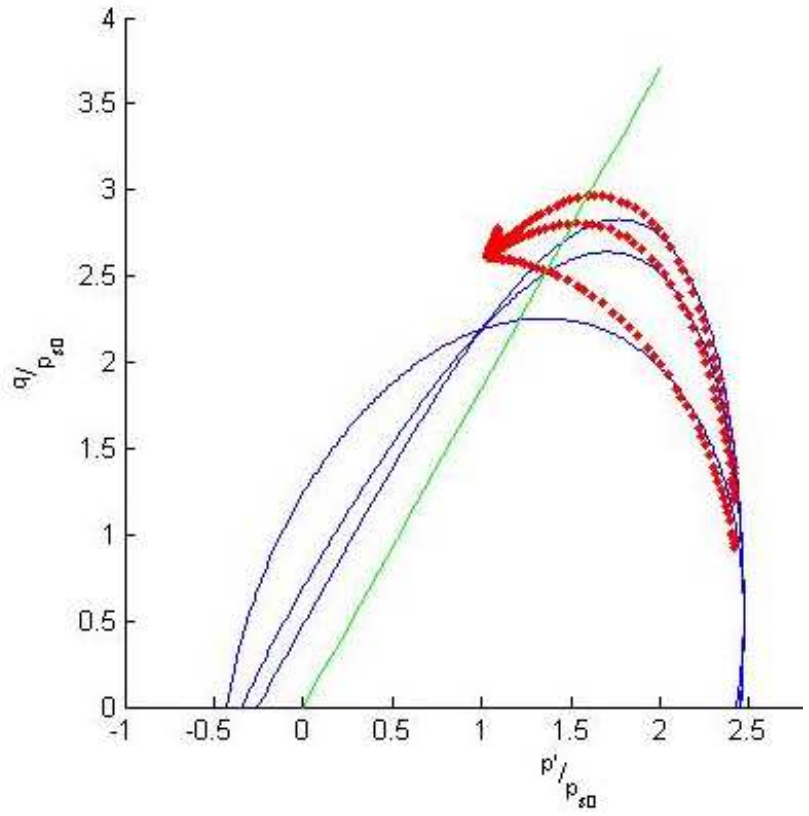

Figure 4.8: Anisotropic yield surface and undrained path when $\theta = 20$ and $\gamma = 0.3,\ 0.5,\ and\ 1$

The combined results of both simulations show that it is necessary to account for the shear induced dilatancy angle as well as cementation in capturing the yield behavior of anisotropic bonded soils.

Chapter 5

Conclusions and Recommendations

5.1 Conclusions

Experimental results on cemented soils have shown that they generally have yield surfaces whose shape and shift in the stress space is dependent on the amount of bonding present. Several models have been proposed in the past based on elastic-plastic framework incorporating ideas of critical state soil mechanics to capture this behavior. In some cases, such models have been found to violate the laws of thermodynamics.

This study presents a thermomechanical model for modeling the yield behavior of cemented soils. The formulation is based on the choice of a free energy function and a dissipation function from the beginning and ensures that no thermodynamic laws are violated. Different choices of the dissipation function are proposed to capture the characteristics of the yield surfaces of bonded soils. The corresponding shapes of the undrained stress path under triaxial loading were also derived. It is shown that the isotropic alpha-gamma model form of the dissipation function can capture the yield loci and the shapes of the undrained stress paths of published laboratory experimental data on cemented soils. Results show that the shape and shift of the yield surfaces are controlled by the model parameters which are functions of cementation. In particular, the parameter γ is found to be directly correlated with the percentage of the cement added.

The study also proposed another model to account for the anisotropy that occurs in natural bonded soils. This model used a coupling between the plastic volumetric and shear strains through a shear dilatancy angle, tan θ. Since quality experimental results on the yield behavior of natural bonded soils are rare, parametric studies were conducted to identify the features of this model. The results show that the rotation of the yield surface is controlled by the parameter, tan θ. In addition it is found that that the shape of the undrained path reaches a peak and progressively reduces to critical state, highlighting the brittle shear behavior of bonded soils. Furthermore, the slope of the critical state line increases with cementation.

5.2 Recommendations for further study

While this study developed the formulations for the plastic yield surface and undrained stress path during deformation, it is recommended that the methodology to be extended to develop a comprehensive constitutive model. This will require the addition of elastic stress strain formulations. The method presented here was restricted to triaxial conditions only, but it can be extended to general 3-D formulations by using suitable invariants as has been done by Collins and Hilder (2002) for natural soils. Once the model is developed, it can also be implemented into a finite element code to simulate field problems. Most importantly, an experimental data based on yield behavior of natural bonded soils should be developed, which will additional insights into the predictions made here.

References

Butterfield,R.A. 1979. Natural compression law for soils (an advance on e -ln (p)) Geotechnique, 29(4), 469-480.

Casagrande, A. 1936. Characteristic of cohesionless soils affecting the stability of slopes and earth fills. Journal of Boston society of civil engineers. Vol.23, p.13

Chazallon, C. and Hicher, P. 1995. An elastoplastic model with damage for bonded geomaterials. Numerical models in geomechnics, ISBN 90 5410 568 2

Collins, I. F. 2005a, Elastic/plastic models for soils and sands. Int.J.Mech Sci. 47, 493-508

Collins, I. F. 2005b. The concept of stored plastic work or frozen elastic energy in soil mechanics. Geotechnique 55 (5), 373-382.

Collins, I.F. and Hilder, T. 2002.A theoretical framework for constructing elastic/plastic constitutive models for triaxial tests. Int. J. Numer. Anal. Methods Geomech. 26, 1313-1347.

Collins, I.F. and Houlsby, G.T. 1997. Application of thermomechanical principles to the modelling of geotechnical materials. Proc. Roy. Soc. Lond. A 453,1975-2001.

Collins, I.F. and Kelly, P.A. 2002. A thermomechanical analysis of a family of soil models. Geotechnique, 52(7), 507-518.

Collins, I., Muhunthan, B., and Qu, B 2008. Thermomechanical State Parameter Models for Sands. Geotechnique [doi: 10.1680/geo.8.P.127]

Collins, I. F. and Muhunthan, B. 2003. On the relationship between stress-dilatancy, anisotropy, and plastic dissipation for granular materials. Geotechnique, 53(7), 611-618.

Gens, A. and Nova, R. 1993. Conceptual bases for a constitutive model for bonded soils and weak rocks. Geotechnical engineering of hard soils, ISBN 90 5410 344 2

Horne, M. 1965. The behavior of an assembly rotund, rigid, cohesionless particles. Part I and II. Proceedings of the Royal society. Vol.286, pp. 62-97.

Houlsby, G.T. and Puzrin, A.M. 2000. A thermomechanical framework for constitutive models for rate-independent dissipative materials. Int. J. Plasticity, 16,1017-1047.

Kasama, K., Ochiai, H. and Yasufuku, N. 2000. On the stress-strain behavior of lightly cemented clay based on an extended critical state concept. Soils and foundation Vol. 40, No. 5, 37-47

Leroueil, S. and Vaughan, P. 1990. The general and congruent effects of structure in natural soils and weak rocks. Geotechnique 40, No. 3, 467-488

Li, X.S. 2007. Thermodynamics-based constitutive framework for unsaturated soils-1: Theory. Geotechnique 57, No 5, 411-422

Luong, M.P. 1986. Characteristic threshold and infrared vibrothermography of sand. Geotechnical Testing J. ASTM, June, 80-86.

Maugin, G.A. 1992. The thermomechanics of plasticity and fracture, Cambridge: Cambridge University Press.

Maugin, G.A. 1999. The thermomechanics of nonlinear irreversible behaviors, an introduction. Singapore: World Scientific Publishing Co.

Muhunthan, B., Chameau, J.L. and Masad, E. 1997. Fabric effects on the yield behavior of soils. Soils and Foundations, 36, No 3, 85-97.

Rajagopal, K.R. and Srinivasa, A.R.(1998). Mechanics of the inelastic behavior of materials, Part II: Inelastic response. Int. J. Plasticity 14, Nos 10-11, 969-995.

Roscoe, K. and Burland, J. 1968. On the generalized stress-strain behavior of 'wet' clay. In Engineering plasticity Cambridge University press, pp. 553-609

Rowe, P.W. 1962.The stress-dilatancy relation for static equilibrium of an assembly of particles in contact. Proc. Roy. Soc.A. 269, 500-527.

Schofield, A. N. and Wroth, C. P. 1968. Critical state soil mechanics, New York London, McGraw-Hill.

Sulem, J. and Ghabezloo, S. 2010. Effect of the volume of the drainage system on the measurement of undrained thermo-poro-elastic parameters. Int J. Rock Mech. Min. Sci., 47(1):60-68

Taylor, D.W. 1948. Fundamentals of soil mechanics. New York, John Wiley.

Ulm, F-J, and Coussy, O. 2003. Mechanics and durability of solids, Vol 1. New Jersey, Prentice Hall.

Vatsala, A., Nova, R. and Srinivasa, M. 2001. Elastoplastic model for cemented soils. J geotech geoenviron eng 127:676-87

Vaunat, J and Gens, A. 2003. Bond degradation and irreversible strains in soft argillaceous rock. Soil mechanics and geotechnical engineering. 479-484

Vogel, C. 2010. Modeling static liquefaction, Final project report, Department of Engineering Science, University of Auckland, NZ.

Yang, C., Huang, M. and Cui, Y. 2011. Constitutive model of unsaturated structured soils under cyclic loading. Taylor and Francis group, London, ISBN 987-0-415-60428-4

Zienkiewicz, O., Chan, A.,Pastor, M., Schrefler, B. and Shiomi, T. 1999. Computational geomechanics with special reference to earthquake engineering. John Wiley and Sons, Inc.

Appendix A

A.1 Isotropic Alpha-Gamma Model Code for bonded Soils

```
% Isotropic Alpha-Gamma Model Code For bonded Soils
% Initialise the global model parametres
global lambda kappa M alpha gamma a1 a2 a3 b1 b3
lambda = 1.166;
kappa = 0.034;
M = 1.49;
alpha = 0.5;
gamma = 0.7;
a1=1-gamma;
a2=0;
a3=2-gamma;
b1=(1-alpha)*M;
b3=M;
egpf=0.5;
n=5;
egp=zeros(n,1);
y=zeros(n,1);
res=500;        % Resolve to 500 points
w=linspace(0,pi,res);   % Yield surface omega
for j = 1:res;
   [p(j) q(j)]= IAGyieldsurf(w(j), 1);
end
% CSL
cr= linspace(0,5,20);
% solve for the stress path
[egp y]= IAGpath(pi/12, [0, egpf]);
% Plot the yield surface, CSL and stress path
figure(1);
hold on
plot(p+1,q)
plot((y(:,1)+y(:,3)), y(:,2), 'r.');
plot(cr, M*cr, 'g');
xlabel('{}^{p''}/{}_{p_{s0}}');
```

```
ylabel('{}^q/{}_{p_{s0}}');
```

A.2 IAGyieldsurf.m

```
function [rho zeta] = IAGyieldsurf(omega,mu)
% Calculate a stress point on the yield surface
global a1 a2 a3 b1 b3
delta = 1-a1*cos(omega)-a2*b1*sin(omega)*cos(omega);
rho = (a2*b3*sin(omega)+a3)*(mu+0.47)*cos(omega)/delta;
zeta = (b1*rho+b3*(mu+0.47))*sin(omega);
```

A.3 IAGpath.m

```
function [egp y]=IAGpath(omega0,tspan)
% Calculates an undrained stress path for the isotropic alpha gamma model
% for bonded soils

% Initial condition (minus omega0)
evp0=0;
mu0=1;
[rho0 zeta0]=IAGyieldsurf(omega0,mu0);
% Solve the ODE
[egp y]= ode45(@IAGMf, tspan, [rho0; zeta0; mu0; omega0; evp0]);
% ----------------------------
% Differential Function
function dy= IAGMf(t, y)
% Fundamental parameters come from the global scope
global lambda kappa a1 a2 a3 b1 b3
% Name variables
rho= y(1);
zeta= y(2);
mu= y(3);
omega= y(4);
evp= y(5);
```

```
% Alpha-Gamma Matrix
%   drho            dzeta           dmu          domega          devp
K=[(1-a1*cos(omega)), -a2*cos(omega), -a3*cos(omega), Afunc(rho,zeta,mu)*sin(omega), 0;
   -b1*sin(omega),    1,          -b3*sin(omega), -Bfunc(rho,mu)*cos(omega),    0;
   0,                 0,          0,              0, Afunc(rho,zeta,mu)*sin(omega);
   0,                 0,          (lambda-kappa), 0,                      -mu-0.47;
   kappa,             0,          kappa,          0,                   rho+mu+0.47];
% Nondimensionalised alpha-gamma RHS
f= [0 0 Bfunc(rho,mu)*cos(omega) 0 0]';
% Calculate differential step
dy=K\f;
```

A.4 Afunc.m

```
function A = Afunc(rho,zeta,mu)
% Calculate the A cofficient given rho, zeta, and mu
global a1 a2 a3
A= a1*rho+a2*zeta+a3*(mu+0.47);
End
```

A.5 Bfunc.m

```
function B = Bfunc(rho,mu)
% Calculate the B coff given rho and mu
global b1 b3
B= b1*rho+b3*(mu+0.47);
End
```